PCCP

ROYAL SOCIETY OF CHEMISTRY

PAPER

View Article Online
View Journal | View Issue

Cite this: *Phys. Chem. Chem. Phys.*, 2024, **26**, 808

Complex oiling-out behavior of procaine with stable and metastable liquid phases†

Da Hye Yang, [a] Francesco Ricci, [b] Fredrik L. Nordstrom [b] and Na Li *[ac]

During the crystallization of a solute from solvent(s), spontaneous liquid–liquid phase separation (LLPS) might occur, under certain conditions. This phenomenon, colloquially referred to as "oiling-out" in the pharmaceutical industry, often leads to undesired outcomes, including undesired particle properties, encrustation, ineffective impurity rejection, and excessively long process time. Therefore, it is critical to understand the thermodynamic driving force and phase boundaries of this phenomenon, such that rational strategies can be developed to avoid oiling-out or minimize its negative impact. In this study, we systematically evaluated the oiling-out behavior of procaine, a low melting point drug, in the solvent systems heptane, and ethanol–heptane as a function of temperature and solvent composition. In the procaine–heptane binary system, we observed a region where the LLPS is metastable with respect to crystallization, which is most commonly observed in the crystallization of modern active pharmaceutical ingredients (APIs); however, we also identified a region of the phase diagram where the LLPS is stable with respect to crystallization, and therefore will persist indefinitely. In the procaine–ethanol–heptane ternary system we identified five different regions, including a homogeneous liquid (L) region, two solid–liquid (SL_I and SL_{II}) regions, a liquid–liquid (L_IL_{II}) region, and a solid–liquid–liquid (SL_IL_{II}) region. The binary and ternary phase diagrams were also predicted using a state-of-the-art thermodynamic model: the SAFT-γ-Mie equation of state, and the results were compared with experimental data. Our findings highlight the complexity of oiling-out behavior. This work also represents a combined modeling and experimental platform to identify phase boundaries that will enable rational selection of strategies to crystallize active pharmaceutical ingredients with oiling-out risks.

Received 23rd September 2023,
Accepted 4th December 2023

DOI: 10.1039/d3cp04622b

rsc.li/pccp

1. Introduction

In pharmaceutical manufacturing, crystallization is a critical step as it affects the purity, polymorphism, particle size and shape, as well as flowability of the active pharmaceutical ingredient (API).[1,2] During crystallization, the drug is typically dissolved in a solvent and then cooled or evaporated to induce crystallization. In the case of an antisolvent crystallization approach, the drug is first dissolved in a solvent in which it has good solubility, and an antisolvent (*i.e.* a liquid that the drug is poorly soluble in, typically also chosen to be miscible with the original solvent) is added to the solution. Regardless of the approach, a supersaturated solution is generated and, either with or without seeding, nucleation and crystal growth occur subsequently. However, an undesired phenomenon, liquid–liquid phase separation (LLPS), also known commonly as oiling-out, might occur during the crystallization process.[3] Oiling-out occurs when the dissolved solute concentration exceeds its miscibility limit with respect to the solvent(s), and a second liquid phase spontaneously separates out from the originally homogeneous solution. Therefore, oiling-out is thermodynamically driven by a liquid–liquid equilibrium (LLE) between a solvent-rich liquid and a solute-rich liquid. Of course, oiling-out can have detrimental effects on API production as it may lead to difficulties in agglomeration and impurity rejection.[3–5] Moreover, long process time and scale-up issues are often associated with systems that oil out. In the most extreme case, oiling-out may actually be stable with respect to crystallization under certain conditions, and hence crystallization would never occur. This possibility is discussed in more detail below.

Several strategies have been used to avoid oiling-out during crystallization. Lowering the level of supersaturation throughout the crystallization,[6,7] seeding at suitable conditions,[6,8–10] nucleation controlling methods such as wet milling and ultrasound,[11] and solvent switch[12,13] are common approaches. For example, Li *et al.* utilized the seeding approach to avoid oiling-out and successfully obtained a stable pyraclostrobin crystalline form with high purity.[14] By changing the ratio of

[a] *Department of Pharmaceutical Sciences, University of Connecticut, Storrs, CT 06269, USA. E-mail: lina@uconn.edu*
[b] *Material & Analytical Sciences, Boehringer-Ingelheim, Ridgefield, CT 06877, USA*
[c] *Institute of Material Science, University of Connecticut, Storrs, CT 06269, USA*

† Electronic supplementary information (ESI) available. See DOI: https://doi.org/10.1039/d3cp04622b

the solvent system, cyclohexane and ethyl acetate,[12] or from acetone/water to 2-propanol/water,[13] oiling-out of a BMS drug candidate and DHDPS (4,4′-dihydroxydiphenylsulfone) was avoided, and crystalline APIs were successfully obtained. However, the selection of such strategies is often based on trial-and-error, and a comprehensive understanding of the oiling-out phenomenon remains lacking.

As mentioned above, there are two distinct classifications of oiling-out behavior within the context of pharmaceutical crystallization.[15] Namely, the LLE (*i.e.*, oiling-out) can either be stable or metastable with respect to the desired solid–liquid equilibrium (*i.e.*, crystallization of the API from the solvent phase). In most pharmaceutically-relevant cases, this liquid–liquid equilibrium is metastable, and therefore the system should eventually evolve to the stable equilibrium state: a slurry of the crystalline solid API and a single liquid phase in which the API concentration is equal to the solid phase's solubility at the given temperature, pressure, and solvent composition. Indeed, for cases in which metastable oiling-out[16] is observed, successful crystallization can often be achieved by proper seeding.[17–19] The alternative case of stable oiling-out[10,20] generally occurs when the crystallization process temperatures approaches the melting point of the solute.[15] This type of stable oiling-out was previously observed in a handful of low melting point compounds, vanillin,[20,21] benzocaine,[22] butyl paraben,[23] ibuprofen,[10] and ketoprofen,[24] under usual crystallization temperatures. Of course, in certain systems one can identify a cross-over between the stable and metastable regimes (*e.g.*, by lowering the temperature such that the stable LLPS becomes metastable with respect to crystallization, as shown in this study). For example, a recent study tried to capture both types of oiling-out behavior for ibuprofen in a 50/50 (v/v) ethanol/water mixture using a kinetic phase diagram,[10] but most cloud points were recorded regardless of the crystalline or amorphous nature of the precipitates. Also, although kinetic phase diagrams are useful with respect of specific processing conditions, the thermodynamic phase boundaries remain unknown.

Therefore, the goal of this study is to systematically examine API oiling-out behavior in single and binary solvent systems as a function of temperature using both experimental and modeling tools. Procaine was selected as a model drug given its low melting point (62 °C[25]) such that the regions for both types of oiling-out may be observed under normal crystallization temperatures. Procaine has only one known polymorph, which enables crystalline solubility determination in different solvent systems. It also has a low crystallization propensity, and thus liquid droplets formed in the metastable oiling-out regime can be experimentally observed before crystallization takes place.[26] Ethanol and heptane were chosen as the solvent and anti-solvent, respectively. The molecular structure of procaine is shown in Fig. 1. Predictions of the relevant thermodynamic phase equilibria (*i.e.* the phase diagrams) are performed with the SAFT-γ-Mie model,[27] a state-of-the-art equation of state (EoS). This model is rigorously grounded in statistical mechanics theory, and can be quite helpful for comparing with the complex phase behavior observed experimentally to obtain better understanding of such phenomena. Moreover, this modeling approach can also be used to aid in solvent selection, thereby screening for solvents which either avoid oiling out, or at least increase the operating range over which oiling-out may be avoided.

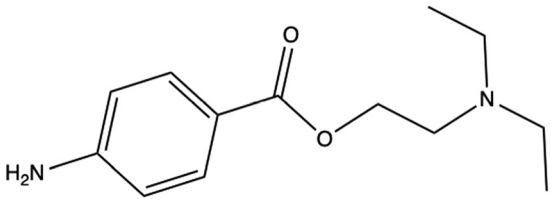

Fig. 1 Chemical structure of procaine.

2. Materials and methods

2.1. Materials

Procaine (>98.0%) was purchased from TCI America (Portland, OR). Ethanol and *n*-heptane were obtained from Thermo Fisher Scientific (Waltham, MA). Reverse osmosis water with a resistivity of 18.2 MΩ cm produced using a water purification system (Microspure UV, Thermo Fisher Scientific, Waltham, USA) was used for all experiments.

2.2. Methods

2.2.1. Instrumentation

X-ray powder diffraction (XRPD). The crystal form of procaine samples was determined by using a Bruker X-ray diffractometer (D2 PHASER, Bruker AXS Inc., Germany) with Cu Kα radiations. Diffractograms were recorded from 5° to 35° (2θ) at a scan rate of 0.02° per step. Samples were equilibrated in their corresponding solvents and analyzed at determined time points to determine polymorphic transition.

Powder X-ray diffractogram for procaine crystals was also calculated based on single crystal data[28] downloaded from the Cambridge Crystallographic Data Centre (CCDC) using Mercury 2022.3.0 (CCDC).

Polarized light microscopy (PLM). Samples were imaged using an Olympus BH-2 microscope equipped with a Qimaging MicroPublisher 3.3 RTV.

High-performance liquid chromatography (HPLC). For systems with small amounts of procaine or solvent where gravimetric measurements may not be accurate, procaine concentration was analyzed using an Agilent 1260 Infinity series high-performance liquid chromatography (HPLC) system (Agilent Technologies, Santa Clara, CA) with an Agilent Eclipse C18 column (particle size: 4.6 μm; length: 150 mm). An isocratic method with mobile phases of ACN and 0.1% (v/v) trifluoracetic acid (TFA) in water at a ratio of 80 : 20 (v/v) was used, and the flow rate was 1 mL min^{-1}. A sample injection volume of 5 μL was used. Procaine was detected at 210 nm.

Gas chromatography–mass spectrometry (GC/MS). GC/MS analysis was performed on a GC/MS 7890A/5975C (Agilent Technologies, Palo Alto, CA) system, with a Restek Rxi-1MS

column (30 m × 0.25 mm × 1 μm). For determination of ethanol and heptane, 0.5 μL of sample was injected at 150 °C with a split ratio of 500 : 1. Oven program was 2 minutes at 35 °C, followed by a 15 °C min^{-1} ramp to 120 °C with no hold.

For instrument control and data acquisition, the MSD ChemStation (Agilent Technologies, Palo Alto, California, USA) software was used. Obtained data were processed using MassHunter (Agilent Technologies, Palo Alto, California, USA). Chromatograms of solvents were obtained in TIC (total ion chromatogram) mode.

2.2.2. Crystalline solubility. The crystalline solubility of procaine in different solvents at various temperatures was determined gravimetrically using the shake flask method. For procaine solubility in neat heptane, an excess amount of crystalline procaine solids was added to the solvent. For solvents with higher ethanol fractions (0.6 and 0.8 v/v ethanol in heptane, as well as neat ethanol), a small amount of solvents were added to excess amount of procaine solids. The mixtures were then stirred and equilibrated for 48 hours with residual solids remaining in solution. Next, the suspension was filtered using a pre-heated 1 mL syringe with a pre-heated 0.22 μm polyvinylidene fluoride (PVDF) filter (MilliporeSigma, Burlington, MA). The filtered solution was added to an empty HPLC vial, which was then placed in a fume hood until all solvents were evaporated. Vial and sample weights were measured before and after drying to calculate the amount of drug and solvent in the saturated drug solution.

2.2.3. Oiling-out limit (OOL)

Antisolvent titration. Antisolvent and reverse-antisolvent titration were used to determine the OOL of procaine in ethanol/heptane mixtures. For the antisolvent titration method, a procaine stock solution was prepared in neat ethanol, and then heptane was gradually added to the stock solution until a cloudy solution was formed, indicating liquid–liquid phase separation. For the reverse antisolvent titration method, the ethanol stock solution was titrated in heptane. The lack of crystallinity was confirmed using PLM.

Briefly, a volume of 0.5 to 5 mL of antisolvent (heptane) or solvent (procaine with ethanol) was prepared in a 20 mL vial. For experiments at room temperature, the solvent or antisolvent was added using a syringe pump at a flow rate of 300 to 800 μL min^{-1} until phase separation was observed. For experiments at temperatures other than room temperature, the vial was placed in a jacketed beaker connected to a circulating water bath to control the temperature. Both the stock solution and the antisolvent were pre-heated or pre-cooled, and then added by hand in small aliquots, until liquid–liquid phase separation occurred.

Heating and cooling experiments. For the procaine–heptane binary system where a second solvent cannot be introduced, direct heating and cooling experiments were performed to determine OOL.

For the heating experiment, 50% (w/w) procaine in heptane was prepared and equilibrated at desired temperatures. For samples that phase separated into two layers of liquids, the sample was allowed to equilibrate for at least 48 hours. Both the upper and lower (heptane-rich and procaine-rich, respectively) layers were then collected using pre-warmed syringes. The amount of procaine in each phase was determined gravimetrically.

For the cooling experiment, heptane solutions with a series of pre-determined procaine concentrations were prepared, and then heated at 65 °C to dissolve all procaine solids. The homogeneous sample was then placed in a jacketed beaker and cooled down to 5 °C. OOL was observed visually, and the onset solution temperature where oil droplets were formed was recorded as the cloud point. The absence of crystallization was confirmed using PLM.

Slurry experiments. To verify lack of polymorphic form transition of procaine, slurry experiments were performed in different solvent systems. Procaine solids were mixed with a small amount of solvent, ethanol or heptane, to form a slurry, which was then allowed to equilibrate at room temperature for 48 hours. The slurry was deposited on a sample holder prior to XRPD analysis.

Slurry experiments were also performed to identify oiling-out phase boundaries and obtain tie-lines. A certain amount of procaine solids was placed in a glass vial, and an ethanol/heptane solvent mixture at pre-determined composition was added at different temperatures. Samples were equilibrated for about 20 minutes, and the appearance was recorded to map out different phase regions on ternary phase diagrams. To obtain tie-lines for regions with liquid–liquid equilibrium and solid–liquid–liquid equilibrium, the samples were allowed to equilibrate for 48 hours. Both liquid phases were then sampled and analyzed using GC/MS to obtain solvent compositions. Procaine concentrations were determined gravimetrically.

2.2.4. Data processing. We converted HPLC results in mg mL^{-1} solution to weight-based concentrations. All experiments were performed in at least triplicates, and data is presented in the form of mean ± standard deviation.

2.2.5. Thermodynamic modeling. The prediction of the various phase equilibria was performed *via* the SAFT-γ-Mie EoS.[27] The SAFT-γ-Mie EoS is part of a class of models based on the statistical associating fluid theory (SAFT),[29,30] which describe the Helmholtz free energy of a pure fluid or fluid mixture as a function of temperature, volume, and mole number(s). Therefore, this approach constitutes a fundamental equation of the form $A(T, V, \{N_i\})$, from which all other thermodynamic properties can be predicted (though for this theory the predictions are restricted to describing fluid phases only). Moreover, this particular variant of the SAFT models employs a group-contribution approach, whereby the molecules are decomposed into segments describing the constituent functional groups. Each segment (*i.e.*, functional group) has several parameters describing properties such as its effective size, as well as various interaction energetics. As the name implies, the SAFT EoS incorporates association effects (*e.g.*, hydrogen bonding, or other short-range interactions) through the use of ''association sites'' attributed to certain segments,

with each site characterized by square-well interaction parameters. We also note that other earlier variants of SAFT have been employed to predict oiling-out;[13,31] however, SAFT-γ-Mie is considered state-of-the-art, and particularly useful due to its group-contribution approach. For a more detailed discussion of SAFT-γ-Mie, the reader is referred to the original papers.[27,32]

The SAFT-γ-Mie model was implemented *via* gPROMS (version 2022.1.0.55261), a software package of Siemens. The model parameters for all the functional groups comprising ethanol and heptane were available in the gPROMS parameter database, and hence those values were used in the predictions. Note that the parameter values for the various SAFT-γ-Mie functional groups in the gPROMS database were determined by regressing experimental data (*e.g.*, vapor pressure and saturated liquid density) from a wide array of chemical species. The solute procaine was then evaluated in the gPROMS Solvent Selection (gSS) module. For our work, we used a beta version of the tool (version 1.0.0-beta 4) provided by the software developers before the official release, as one of the authors was actively involved in early evaluation of the tool, see the ESI† for more details. In the gSS module, the required input data for the solute are: the 2D molecular structure (*via* a SMILES string), and information about the crystal polymorph of interest (*i.e.*, the melting temperature and enthalpy of fusion). The tool then evaluates whether the SAFT-γ-Mie parameters for each of the solute's component functional groups are all available within the gPROMS parameter database. If the parameters of the solute are all indeed "covered" by the database, one may proceed directly to prediction of solubility, as well as other phase equilibria. If the solute is not "covered" then one must regress the solute parameters to experimental solubility data as described in the below.

Database model. Initial assessment in the gSS tool confirmed that the functional groups comprising procaine are available in the gPROMS database. Therefore, following the methods described below, one could proceed to directly predict the relevant LLE and solid–liquid equilibrium (SLE) using these parameters, and also the melting temperature and enthalpy of fusion of the polymorph of interest. We used melting-point values which were measured in-house *via* DSC at a heating rate of 10 degrees per minute, with a melting point of 60.24 °C, and enthalpy of fusion of 104.87 J g^{-1}. This approach of describing procaine's interaction parameters *via* the gPROMS database will henceforth be referred to as the *database model* for brevity. However, as will be discussed in the Results section, relying on these database parameter values for the procaine functional groups did not always provide sufficient prediction accuracy, particularly in the procaine–heptane binary system.

Molecular model (regressed model). We also employed an alternative approach whereby the solute (procaine) is treated as a "molecular model", meaning that the entire solute molecule is designated as a single new functional group. The only further user-input for this model definition is a specification of how many association sites are present in the overall molecular model. The association sites are sub-divided into "electron donor" and "electron acceptor" sites, and the choice of how many of each is made judiciously based on the functional groups comprising the solute and also, from a practical perspective, on the amount of solubility data available for regressing the parameters. For the molecular model of procaine, we defined 2 donors and 2 acceptors. The gSS tool was then used to determine procaine self-interaction parameters, as well as certain cross-interaction parameters between procaine and the solvent functional groups, by fitting the model to experimental crystalline solubility data, which we measured in pure solvents at varying temperature: ethanol (4, 10, and 25 °C), heptane (4, 10, 25, 37, and 50 °C), and water (4, 10, 25, 37, and 50 °C). Because this is a regression of crystalline solubility data, the aforementioned melting data for the crystalline polymorph of interest was also needed. Note, the gSS software estimates the solid-phase activity (*i.e.*, chemical potential) of the solute based only on this melting data; it makes the common assumption neglecting the isobaric heat capacity difference between the solid and subcooled liquid phases of the solute (ΔC_P) present in the full expression.

This approach will be referred to as the *molecular model* or *regressed model* approach in the discussion below. For more details, including regressed model parameters, refer to the ESI.†

For both the database model and molecular model approach, we then used gPROMS Properties to construct the phase diagrams by performing a series of isothermal–isobaric (T, P) flash calculations with varying temperature and/or feed composition. In these calculations, SAFT-γ-Mie was used to describe any fluid phases (*i.e.*, gas or liquid), and it was assumed that only pure solid phases could form, which is in-line with experimental observation in the systems studied. The flash algorithm then determines the stable phase(s) present at equilibrium *via* Gibbs free energy minimization. For conditions where the LLE was metastable with respect to the SLE (crystallization of procaine), the solid phase of procaine could be removed from consideration in the algorithm, thereby allowing the flash to "ignore" the stable SLE and converge to the metastable LLE, thus facilitating a plot of the of the LLE binodal curve in the metastable region.

3. Results

3.1. Crystalline solubility

The crystalline solubility of procaine at various temperatures is summarized in Table 1. Experiments were not carried out at 55 °C due to spontaneous LLPS. In all cases, the solid phase was confirmed to be the same crystalline form as the starting procaine solids as shown in Fig. 2, agreeing with the calculated powder pattern.

As expected, the crystalline solubility of procaine increased with increasing temperature and ethanol fraction. LLPS was observed in mixture solvents with ethanol volume fractions of 0.2 and 0.4. Nevertheless, crystalline solids were obtained in presence of higher amount of ethanol, enabling crystalline solubility measurements at ethanol volume fractions of 0.6, 0.8, and 1 (solvent compositions expressed on a solute-free basis).

Table 1 Crystalline solubility of procaine in ethanol/heptane solvent systems

Temperature	Ethanol fraction in heptane (v/v)	Crystalline solubility (mg g^{-1} solvent)
277.15 K (4 °C)	0	0.8546 ± 0.3231
	0.2	LLPS
	0.4	LLPS
	0.6	492.9 ± 26.3
	0.8	968.3 ± 41.2
	1	1560 ± 4
283.15 K (10 °C)	0	1.454 ± 0.062
	0.2	LLPS
	0.4	LLPS
	0.6	700.4 ± 31.3
	0.8	1239 ± 19
	1	1940 ± 41
298.15 K (25 °C)	0	4.613 ± 0.068
	0.2	LLPS
	0.4	LLPS
	0.6	1814 ± 295
	0.8	3680 ± 258
	1	5837 ± 230
310.15 K (37 °C)	0	11.06 ± 0.25
	0.2	LLPS
	0.4	LLPS
	0.6	11319 ± 4733
	0.8	13151 ± 4816
	1	NA

NA: values not obtained due to extremely high procaine solubility.

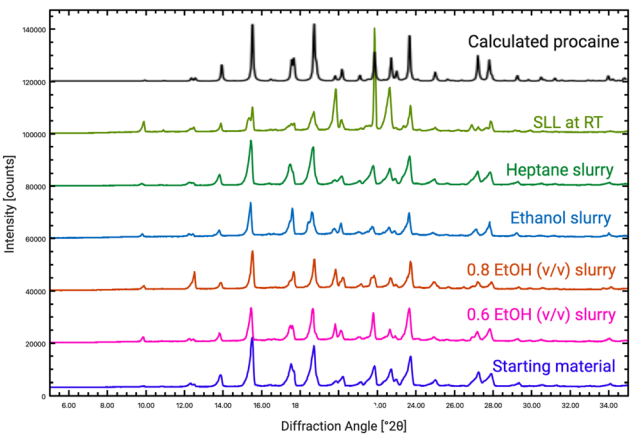

Fig. 2 X-ray powder diffractograms of procaine slurry in different solvents at room temperature for 48 hours.

3.2. Procaine–heptane binary system

The crystalline solubility and OOLs of procaine in heptane are summarized in Fig. 3.

Two types of oiling-out behavior, stable and metastable LLE, were observed. Metastable OOLs were determined using cooling experiments. Upon cooling, small procaine oil droplets spontaneously precipitated out from solution at certain temperatures, and a cloudy solution was observed (Fig. 4A). The LLPS is metastable with respect to crystallization below the transition temperature of approximately 55 °C, where the crystalline solubility curve and the LLE binodal curve cross. Above the transition temperature, the LLE binodal region becomes stable with respect to crystallization. This could be reproduced by heating the crystalline solids suspended in heptane. Large oil droplets were observed (image 1 in Fig. 3A). If a large amount of procaine was added, oil droplets coalesced quickly and formed a layer of immiscible liquid (image 2 in Fig. 3A). The compositions of both layers of liquids, after equilibrium, were analyzed gravimetrically and are shown in Fig. 3, corresponding to the two ends of the miscibility gap.

The phase domains of procaine in heptane are shown schematically in Fig. 4A. The crystalline and liquid phases formed were confirmed using PLM (Fig. 4B and C). At the aforementioned transition temperature (≈55 °C) separating the metastable and stable LLE regions, there is a line of three-phase coexistence between the two liquid phases and the pure crystalline solid procaine. Therefore, we denote this temperature T_{SLLE}, due to the solid–liquid–liquid equilibrium along this line. In this condition of SLLE, the chemical potential of procaine in the two liquid phases is the same and equals that of the crystal phase of procaine, and the chemical potential of heptane is equal in both liquid phases. In the particular scenario schematically shown in Fig. 4, as the temperature is raised, the mutual miscibility of both species increases until an upper critical solution temperature (UCST) is reached, above which the components form a single homogeneous liquid phase over all compositions.

The procaine-rich liquid phase was saturated with about 2.4% (w/w) heptane at T_{SLLE} (Fig. 3). Below the T_{SLLE}, LLE is metastable relative to solid–liquid equilibrium (SLE), and *vice versa*, above T_{SLLE}, the solid phase is metastable relative to the two liquid phases when operating between the LLE binodals. The melting point of neat procaine solids was reported to be 62 °C,[25] and hence stable LLPS only occurs at temperatures close to the melting point in this system. This feature, if generalizable to other pharmaceutical and organic compounds in a single solvent, may render stable LLPS difficult to identify, because typical APIs tend to exhibit melting points closer to 200 °C, and therefore the detection and measurement of stable LLPS can be practically challenging given the relatively-low boiling points of most solvents at atmospheric conditions. Moreover, there are systems for which the LLE binodal never crosses the solubility curve, and hence stable LLE does not exist at any point in the phase space.

Referring to Fig. 4, we also note that a SLE region is expected at high procaine fractions between the T_{SLLE} and pure procaine's melting point. However, due to the extremely high procaine solubility and difficulties identifying whether a homogeneous liquid phase was formed in the small amount of liquid phase, phase boundaries could not be established experimentally.

In aqueous solutions, the onset LLPS concentration is approximated as the aqueous "amorphous solubility" of a poorly soluble drug.[33–35] Usually, amorphous solids are thought to be less stable than its crystalline counterpart. However, if the temperature is kept above the T_{SLLE} of the immiscible liquid phase, the amorphous (liquid) form becomes thermodynamically stable. This was previously observed in nicardipine, where

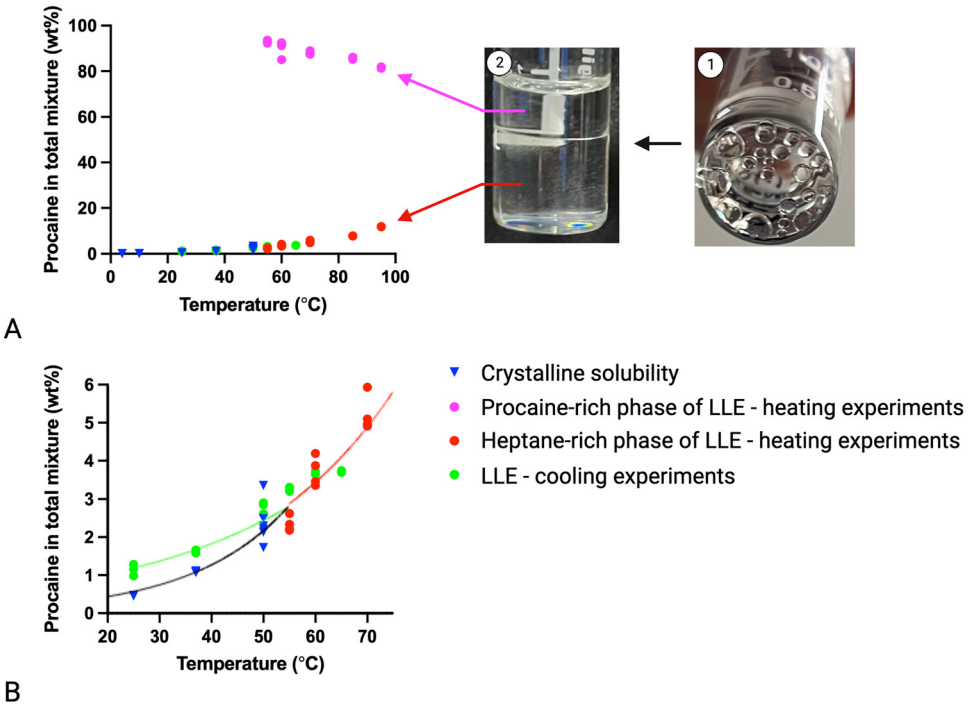

Fig. 3 Procaine–heptane binary phase diagram, including crystalline solubility, stable LLE (observed during both heating and cooling), and metastable LLE (observed during cooling): (A) the complete phase diagram with images showing stable LLE in HPLC vials, and (B) a zoomed-in diagram showing differences between crystalline solubility and metastable LLE, as well as the crossover temperature (T_{SLLE}), above which the LLE becomes stable with respect to crystallization. Lines are fitted exponential curves for the metastable LLE, stable LLE, and SLE phase boundaries.

spontaneous crystalline-to-amorphous (liquid) transition occurred by directly putting the crystalline solid in water at room tempreautre.[36] Although neat nicardipine has a melting point of 115 °C (experimentally measured in-house), the transition temperate was substantially lower in this particular case, possibly due to saturation with water or the presence of impurities. In this study, a similar spontaneous solid-to-liquid transition was also observed for procaine in water at 55 °C. However, investigations were not carried out in aqueous systems due to extensive degradation of procaine in the aqueous environment (data not shown).

3.3. Procaine–ethanol–heptane ternary system

The phase behavior of procaine in ethanol/heptane mixture solvents are summarized in ternary phase diagrams shown in Fig. 5. Data obtained through different experimental methods were used to construct phase boundaries. Based on experimental data, schematics of the ternary phase diagrams at temperatures below and at 55 °C are shown in Fig. 6. To improve readability, areas of different phase regions in the schematic are exaggerated and not proportional to actual data.

At temperatures below 55 °C, a total of five regions were observed: a homogeneous liquid (L) region, a liquid–liquid (L_IL_{II}) region, a solid–liquid–liquid (SL_IL_{II}) region, and two solid–liquid (SL_I and SL_{II}) regions. The areas of both solid-containing phases, SL_I and SL_IL_{II}, decreased with increasing temperature, indicating increasing procaine solubility with temperature (Fig. 7). The area of the L_IL_{II} region increased with increasing temperature. At 55 °C, the solid phase was not observed, leaving only the L and L_IL_{II} regions. This is consistent with the transition temperature observed in procaine–heptane binary systems. In the presence of ethanol, stable liquid–liquid phase separation occurred at all temperatures from 4–55 °C, well below the drug's melting point. Indeed, at 4 °C the area of the L_IL_{II} region is still large in the phase diagram, and is not expected to diminish soon as temperature continues to drop.

The green squares obtained *via* antisolvent titration are considered as binodal phase boundaries. It intercepted with the crystalline solubility (red circles) and formed the phase boundary separating the homogeneous liquid phase from SL_I and L_IL_{II} phases. The SL_IL_{II}, SL_I, and L_IL_{II} regions were identified using slurry experiments and tie-lines. At low ethanol concentrations, a second SL phase region (SL_{II}) was also confirmed (blue triangles, more clearly shown in Fig. 5D). Tie-lines were determined by compositional analysis after being equilibrated for 48 h, gravimetrically for procaine and GC/MS for ethanol and heptane, of the two immiscible liquid layers obtained in L_IL_{II} and SL_IL_{II} regions. In the SL_IL_{II} region, since the degrees of freedom of this system is 0 when temperature and pressure are fixed (DOF = components − phases + 2 = 3 − 3 + 2 = 2, and with T & P fixed, DOF = 0), the compositions of all three phases (the crystalline solid, and the two liquid layers) remain identical regardless of the starting composition. This is confirmed by the overlapping red tie-lines obtained. These tie-lines also serve as the phase boundary between SL_IL_{II} and L_IL_{II} regions, and agree well with the slurry data shown in purple and green triangles. The solid phase is the pure procaine

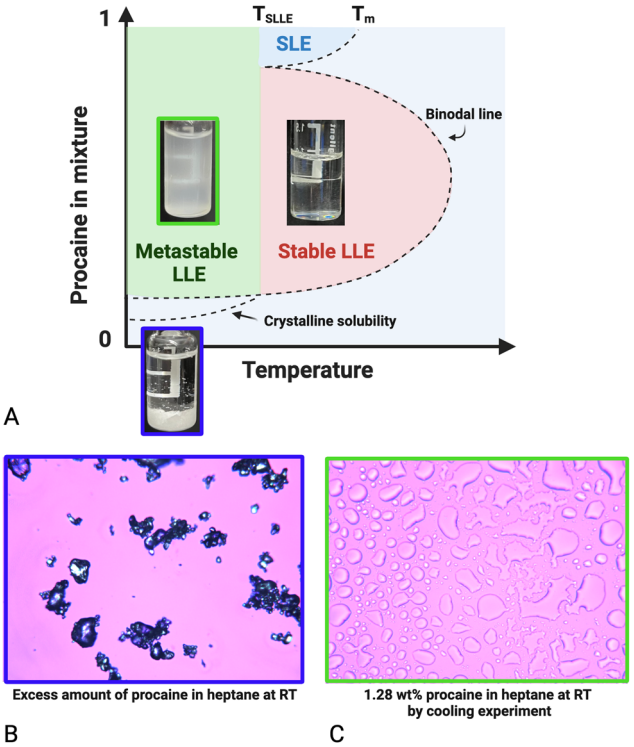

Fig. 4 Phase behavior of procaine in heptane: (A) schematic showing the procaine phase behavior in solution, and PLM images of (B) a suspension containing the crystalline drug at room temperature, and (C) a solution that oiled out at room temperature. Pictures are color coded to show sample appearance and locations in the phase diagram.

crystal, corresponding to the procaine vertex in the SL_IL_{II} region. There were slight discrepancies between the slurry (triangles) and crystalline solubility data (red circles). This is possibly because data obtained using different experimental methods were compared. Immiscible liquid layers formed in the L_IL_{II} region have different compositions, and this is confirmed by different tie-lines obtained in the two-phase region. These tie-lines also correspond well with the L/L_IL_{II} phase boundaries obtained.

To confirm the complex phase behavior of procaine, slurry experiments were performed at 4 °C, and the appearance of samples were recorded.

Fig. 8 shows the visual appearance of samples in four different phase regions. Starting from 50% procaine in heptane, different phase regions were observed sequentially by gradually adding ethanol to the system. The system initially existed as a mixture of crystalline procaine solids and heptane-rich liquid. With more ethanol added, the system transitioned to a solid–liquid–liquid equilibrium region, where crystalline solid procaine coexists with two immiscible liquid phases, one solvent-rich and the other procaine-rich. This condition is thermodynamically stable (SL_IL_{II} was maintained after equilibrium for 48 hours, data shown as tie-lines in Fig. 5A–C). Subsequently, the system entered a liquid–liquid region, where all procaine solids were dissolved. We performed seeding experiments for the sample showing two liquid phases. Procaine solids dissolved completely and two layers of liquids remained, confirming the thermodynamic stability of both liquid phases. With more ethanol added, a transient solid–liquid mixture was observed. After a few days, the sample reached thermodynamic equilibrium and became a homogeneous liquid, with the procaine solids completely dissolved.

3.4. Thermodynamic modelling of phase equilibria

In this study, it was observed that relying on the database model for procaine provided mixed results. In the procaine–ethanol system, the prediction of crystalline procaine solubility was quite reasonable, with errors ranging from 11–46% as compared to the three experimental solubility data at 4, 10, and 25 °C. No oiling-out was predicted or experimentally observed in procaine–ethanol over the temperature range of interest. However, for the procaine–heptane system, it was found that the database model did not exhibit sufficient accuracy, with both the crystalline solubility and oiling out (*i.e.*, LLE binodal) predictions being approximately one order of magnitude under-predicted *vs.* experimental data (for more information consult the ESI†). The molecular model was therefore also employed in order to assess its relative accuracy in prediction of the various phase equilibria when one has access to crystalline solubility data for the solute of interest. The molecular model (see ESI† for more details) fit the regressed data very well, when compared to solubility models commonly employed across the pharmaceutical industry,[37] with an average deviation between experimental and predicted data of 6.7%, and a median deviation of only 3.1%. As with the database model, the molecular model did not predict oiling-out in procaine–ethanol over the temperature range of interest, which is in line with experimental observation.

3.4.1. Procaine–heptane. The molecular model prediction of the procaine–heptane phase diagram at 1 atm is illustrated in Fig. 9. Once again, as this is a molecular model, the SLE data (blue circles) were used to regress the procaine parameters, and an excellent fit is observed.

The oiling-out data is generally in very good agreement with the predicted LLE binodal for the heptane-rich liquid, despite that this data was not incorporated in the model regression. However, the procaine-rich liquid (*i.e.*, the oil phase) is predicted to be approximately pure procaine, and the predicted crossover temperature between the LLE binodal and the solubility curve is 60.24 °C, identical to pure procaine melting point used as model input. Hence, the model over-predicts T_{SLLE}, (experimentally observed as ~55 °C) and estimates that it's effectively equal to the melting point of the pure solid. We also note that the procaine-rich side of the predicted LLE binodal appears to be highly insensitive to temperature, and therefore an UCST was not predicted to occur as it was pre-empted by the formation of the vapor phase at 1 atm, hence why the binodal abruptly ends in the phase diagram.

Despite these discrepancies with experiment, the accuracy with which the LLE binodal is predicted relative to the high-fidelity solubility curve underscores the potential utility of this approach to at the very least serve as a solvent screening tool for identifying systems with high oiling out propensity. Indeed, the

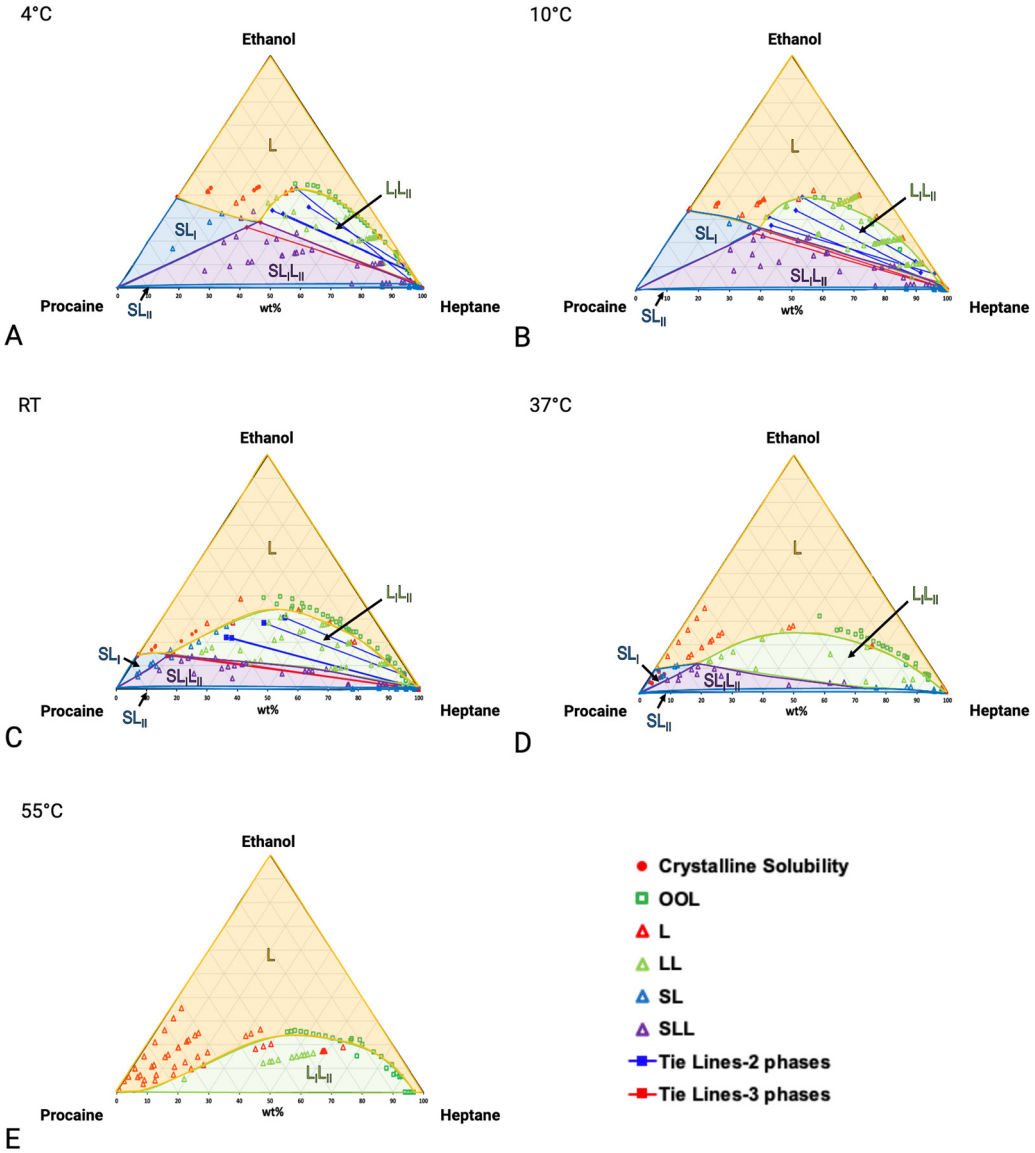

Fig. 5 Ternary phase diagrams of procaine–ethanol–heptane at various temperatures: (A) 4 °C, (B) 10 °C, (C) RT, (D) 37 °C, and (E) 55 °C.

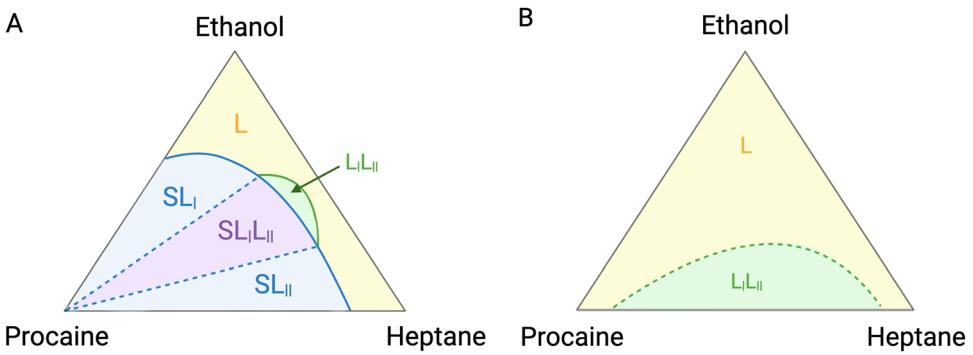

Fig. 6 Schematics of ternary phase diagrams (A) below T_{SLLE}, with all phase regions exaggerated for illustration purposes, and (B) above T_{SLLE}.

LLE binodal results for this particular system are so accurate in the solvent-rich liquid region that one may even be able to use such predictions as a first-pass methodology for *in silico* crystallization process design.

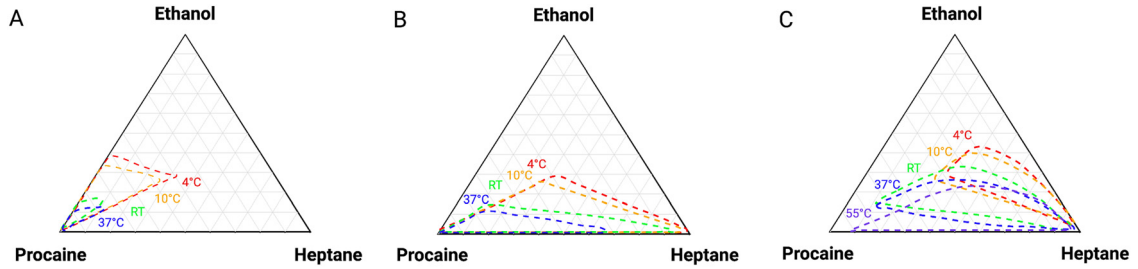

Fig. 7 Evolution of different phases as a function of temperature: (A) SL_I region, (B) SL_IL_{II} region, and (C) L_IL_{II} region.

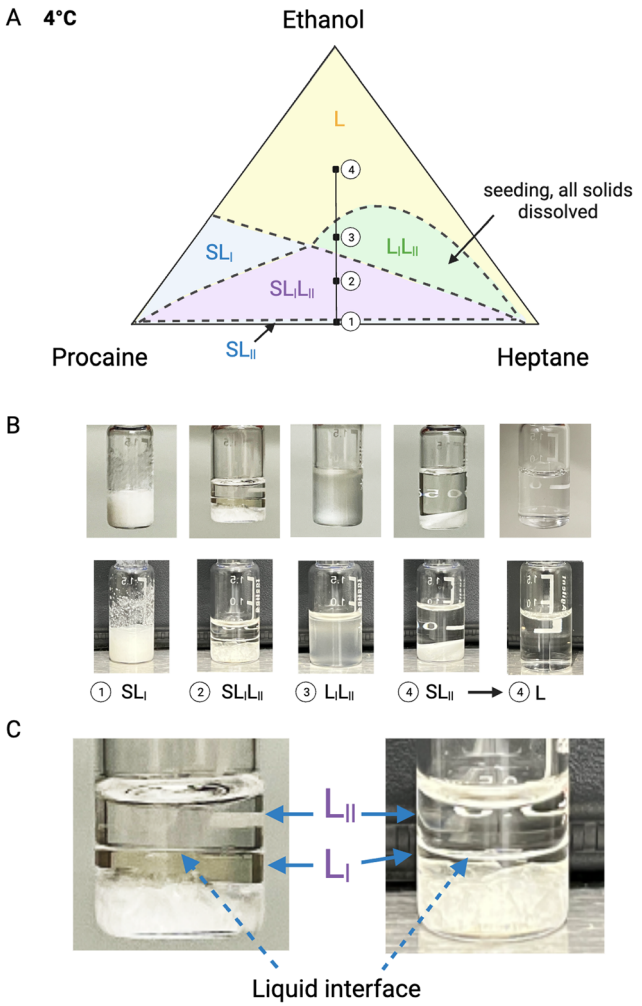

Fig. 8 Different phase regions observed during solvent addition starting from 50% procaine in heptane: (A) phase diagram showing the path, (B) images with bright and dark backgrounds showing co-existence of multiple phases, and (C) close-ups of SL_IL_{II} images to show the liquid interface.

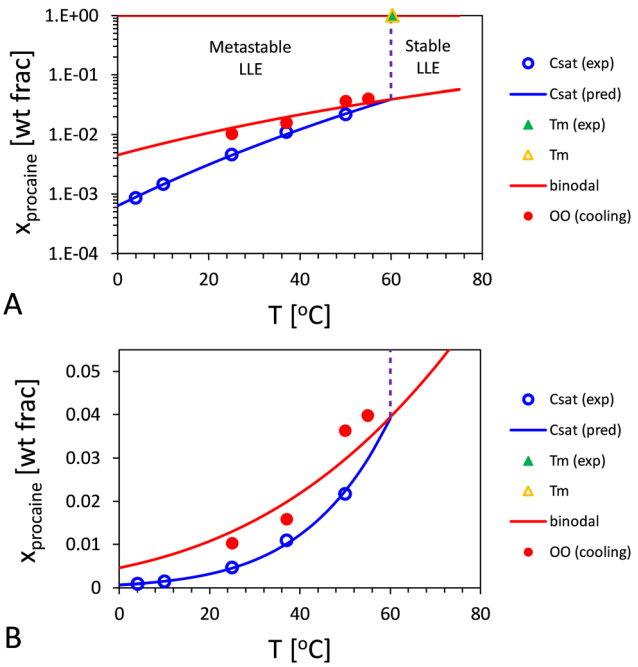

Fig. 9 Molecular model prediction of procaine–heptane phase diagram at 1 atm: (A) semi-log plot to capture both sides of the LLE binodal, and (B) linear plot zoomed-in to observe the accuracy of predicting LLE and SLE, as well as the crossover temperature, above-which the LLE becomes stable.

3.4.2. Procaine–ethanol–heptane. The molecular model predictions for the ternary procaine–ethanol–heptane system are shown in Fig. 10 below. As compared to the experimental data in Fig. 5, the model qualitatively predicts all of the expected phase regions. Note that, we here adopt the notation L_I and L_{II} to clearly differentiate the ethanol/procaine-rich liquid phase and the heptane-rich liquid phase, respectively. While the solubility curves for the ethanol–procaine and heptane–procaine binary systems are quite accurate as previously mentioned, we see a quantitative discrepancy in the width of the SL_I region, as well as the overall area and *T*-sensitivity of the L_IL_{II} region. By 55 °C, the SL_IL_{II} is predicted to be almost completely gone.

Interestingly, the database model does a relatively good job of predicting the phase diagram in this system. Referring to Fig. 11 it is apparent that, although the solubilities in ethanol–procaine and heptane–procaine are less accurate, the overall qualitative features of the phase diagram are comparable to, and in some ways in better agreement with, the experimental results reported in Fig. 5. In particular, the width of the SL_I region, as well as the area and *T*-sensitivity of the L_IL_{II} regions seem better-aligned with experiment when relying on the database parameters to describe procaine. This is particularly

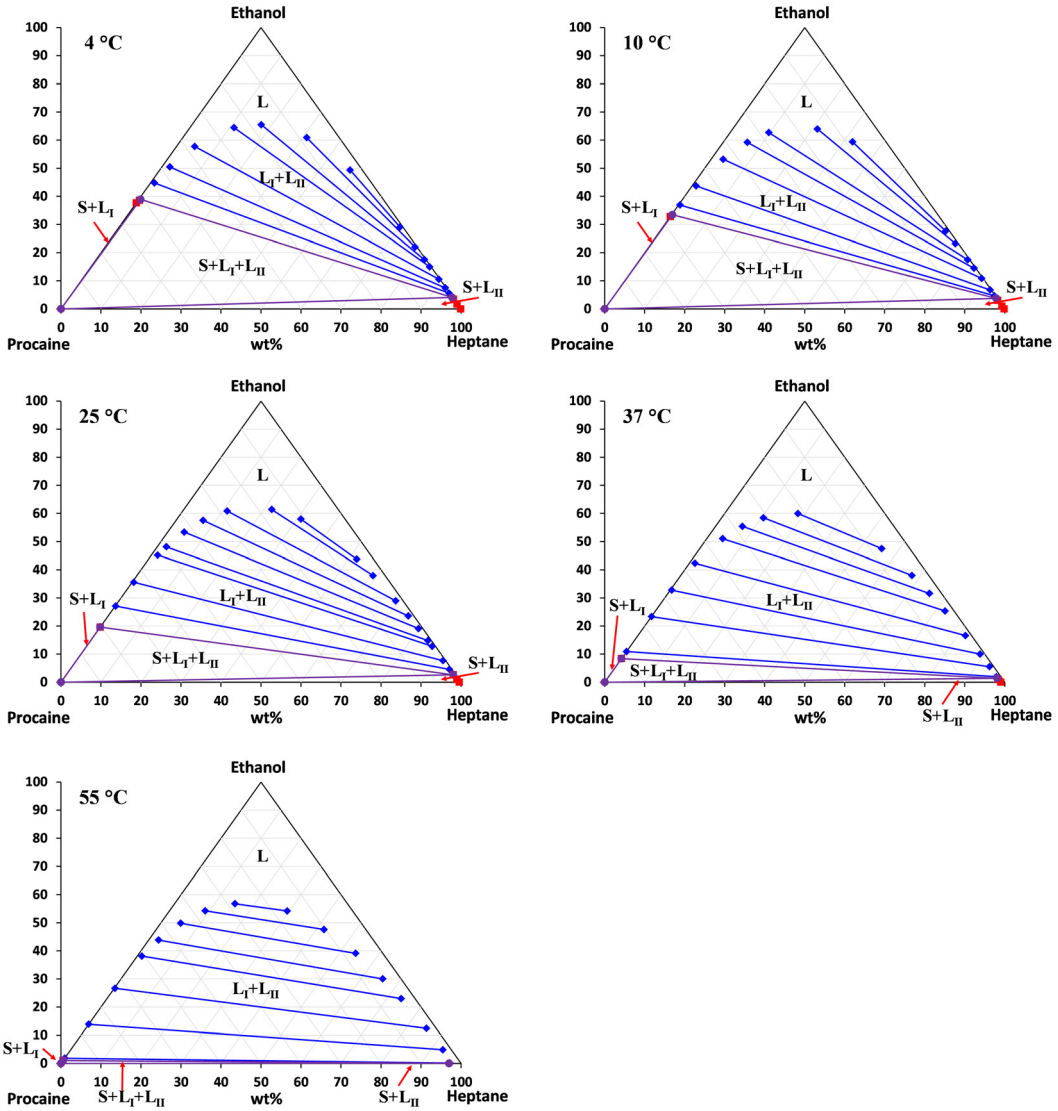

Fig. 10 Molecular model prediction of procaine–ethanol–heptane phase diagram at 1 atm and temperatures (4, 10, 25, 37, and 55 °C). The procaine/ethanol-rich liquid and heptane-rich liquid are denoted as L_I and L_{II}, respectively, for ease of differentiation between the various regions of the phase diagram.

noteworthy, since no data specific to procaine was used in generating these phase diagrams aside from the melting point temperature and enthalpy of fusion necessary to describe its solid state, yet this complexity of phase behavior was still qualitatively reproduced.

Hence, both the molecular model and database model are able to qualitatively reproduce the complex phase behavior exhibited in this system, with each approach showing better quantitative agreement with different aspects of the phase diagram. Perhaps additional experimental solubility data, or the ability to regress solubility data from binary and higher-order solvent systems (which the gSS tool currently does not facilitate) could lead to the molecular model gaining a significant advantage over the database model in general; however, this remains speculative at present.

4. Discussion

4.1. Stable and metastable liquid–liquid phase separation (LLPS)

Two types of oiling-out behavior, stable and metastable LLPS, were observed in this study. Metastable LLPS occurs in supersaturated solutions, in which a second liquid phase separates from the solution when the drug concentration exceeds its miscibility gap with the solvents. If the amount of solvent in the oil phase is sufficiently low, the onset concentration at which metastable LLPS occurs is approximated as the "amorphous solubility" of the drug. Because both liquid phases are supersaturated, there is a risk of crystallization in both phases.

In a binary drug-solvent system exhibiting similar behaviors found with procaine–heptane, the transition temperature (T_{SLLE}) separates metastable LLE and stable LLE. However, with the

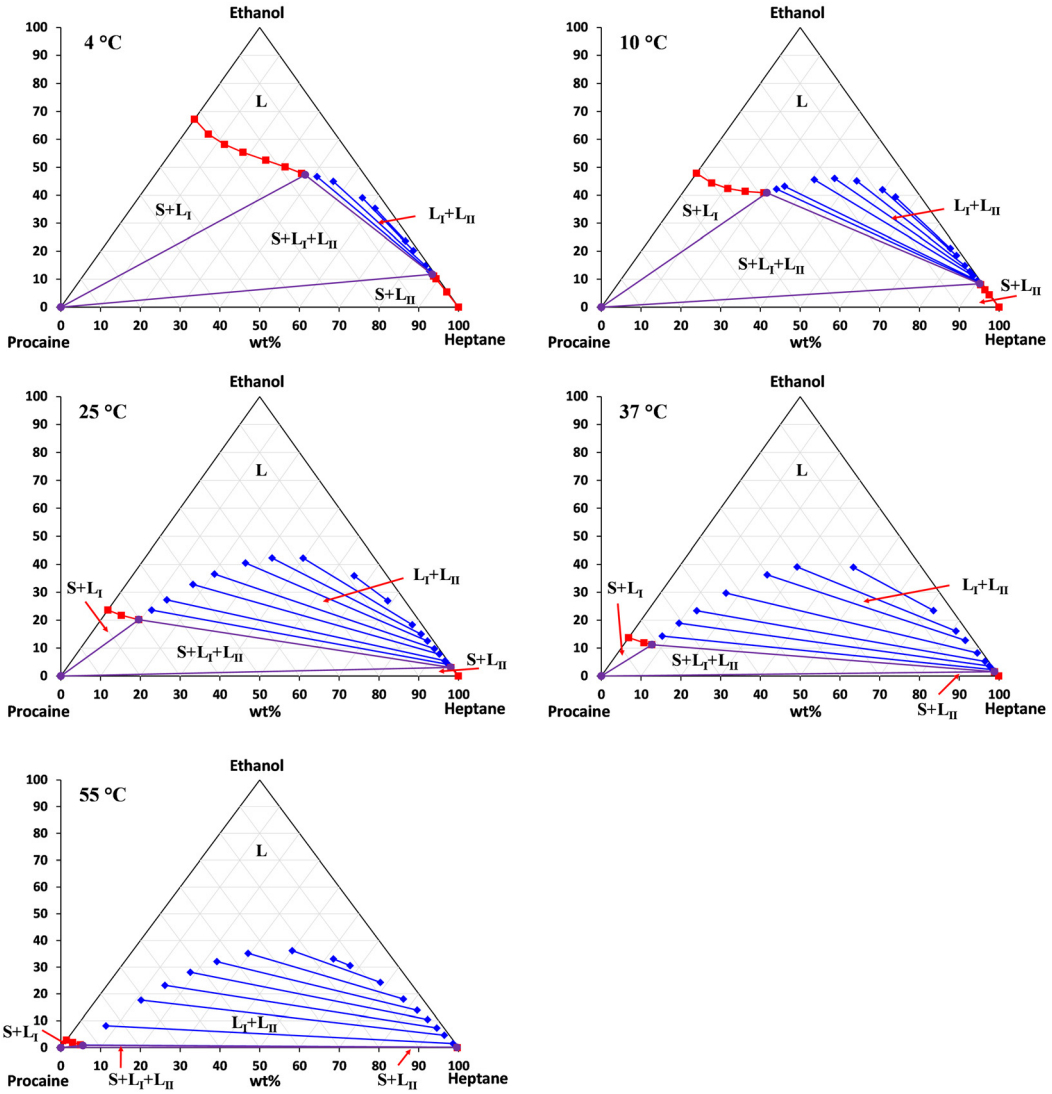

Fig. 11 Database model prediction of procaine–ethanol–heptane phase diagram at 1 atm and temperatures (4, 10, 25, 37, and 55 °C). The procaine/ethanol-rich liquid and heptane-rich liquid are denoted as L_I and L_{II}, respectively, for ease of differentiation between the various regions of the phase diagram.

addition of a second solvent it is possible for stable LLPS to occur at temperatures well below the transition temperature observed in a single solvent. For example, the transition temperature was observed to be approximately 55 °C for procaine–heptane. However, with the addition of ethanol to the system, we also observed states in which two liquid phases coexist at equilibrium (as both L_IL_{II} and SL_IL_{II} coexistence) between 4 and 37 °C. In the SL_IL_{II} region, the liquid phases formed are in equilibrium with the procaine crystal and therefore are thermodynamically stable. The L_IL_{II} region is also thermodynamically stable as it is outside of the crystalline solubility phase boundary.

As demonstrated in the schematic shown in Fig. 12A and B, the liquid and solid–liquid regions are separated by the crystalline solubility of the drug, whereas the liquid and liquid–liquid regions are separated by the binodal phase boundary. The area between binodal and crystalline solubility is the metastable region, where a supersaturated homogeneous liquid can crystallize and reach the thermodynamically stable state. For procaine, however, the binodal is shifted to compositions outside the crystalline solubility boundary. In this case, the LLE becomes thermodynamically stable. In Fig. 12C and D, we illustrate an example of predicting the entirety of the LLE domain in the procaine–ethanol–heptane ternary system, spanning regions where LLE is globally stable and also regions where it is metastable with respect to other equilibria. In Fig. 12D only the predicted stable equilibria are shown. In contrast, in Fig. 12C the entire LLE binodal is plotted, even into the region where LLE is not the globally stable equilibrium state. Similarly, by comparison of Fig. 12C and D, one can see that the LLE is only stable when the LLE binodal crosses the crystalline solubility curve, otherwise the stable equilibrium state must contain the crystalline solid phase (*i.e., via* SL_I, SL_{II}, or SL_IL_{II} equilibrium). This type of analysis could serve a

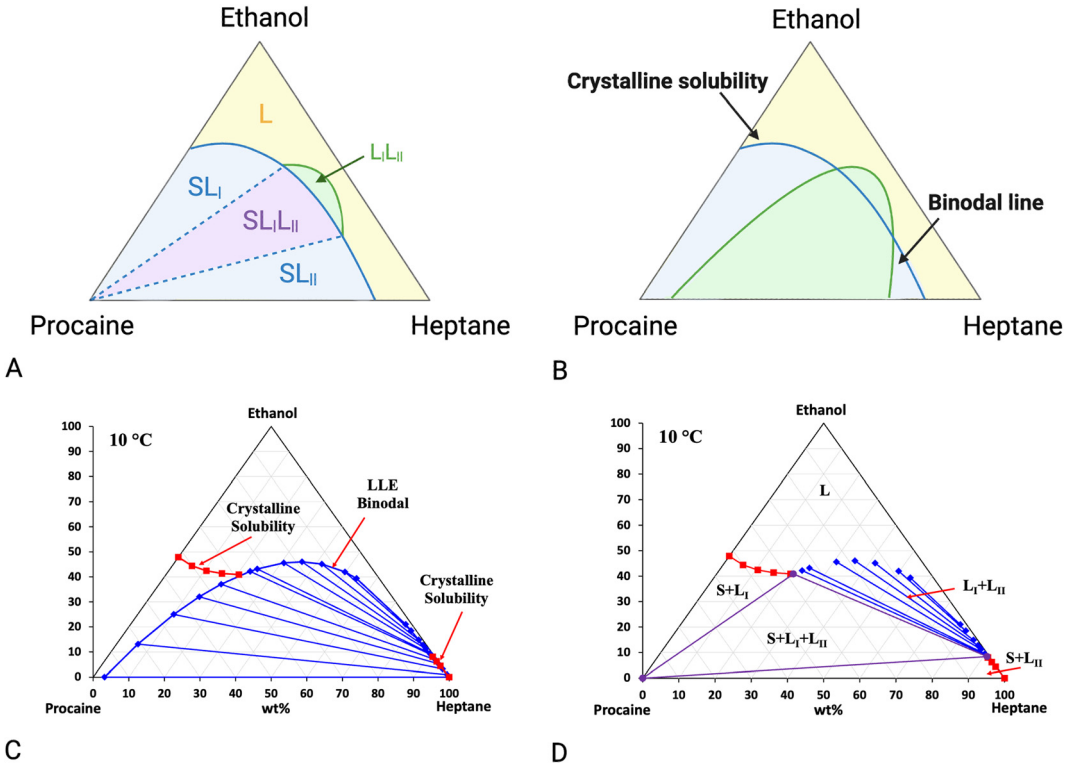

Fig. 12 Schematics showing: (A) different phase regions, (B) the crystalline solubility and binodal line, and phase diagrams illustrating the simultaneous evaluation of stable and metastable equilibria, as predicted by the SAFT-γ-Mie EoS. (C) The LLE region is plotted in its entirety (generated by excluding the solid procaine phase from the (*T*, *P*) flash), and the binodal curve encapsulating this region is explicitly shown for clarity, and (D) Stable equilibria only. Note, when the amount of procaine exceeds the crystalline solubility curve, the solid phase must be present at equilibrium, and hence LLE becomes metastable with respect to other equilibria.

practical purpose for the avoidance of oiling out. For example, at the temperature shown in Fig. 12C and D, a non-negligible portion of the SL_I region, and the entirety of the SL_{II} region are overlapped by the metastable LLE dome, hence oiling out might occur in those overlapping regions before the formation of the solid phase. In the SL_IL_{II} region, the two liquid phases would persist indefinitely, even after the formation of the solid phase.

4.2. Implications to pharmaceutical development

Understanding how stable and metastable LLPS occur is crucial for pharmaceutical applications whenever the drug is in contact with a solvent(s). For example, solid form screenings, such as polymorph, salt, and co-crystal screening, are typically carried out using a variety of solvents in early- to mid-development to find a commercially viable solid form of the API. However, the occurrence of LLPS can negatively affect the success rate of these screens, as it limits the available solvent space and operational flexibility. This is particularly true in salt and co-crystal screening when anti-solvents are added to a dissolved solution comprising the API and counterion or co-former to generate supersaturation for a presumed salt or co-crystal. In these cases, the allowable supersaturation ratio is often limited by LLPS, which slows down the rate of crystallization of any new potential crystalline form.

From an industrial processing perspective, LLPS can also be highly problematic during the crystallization process, where the API is isolated with controlled purity, crystal form, particle properties, and yield. This of course also extends to the isolation of intermediates and other crystalline molecular compounds. Unless for specialized applications, such as spherical agglomeration, the solvent system chosen for crystallization must not yield thermodynamically stable LLPS at any process conditions. The formation of metastable LLPS can also cause issues, even though it is temporary and tends to disappear as the crystal phase nucleates, or is introduced by seeding, and the supersaturation is consumed. This is due to the significant challenges in controlling the final quality attributes of the API when crystallization takes place in two liquid phases that may or may not mix well at scale. Therefore, it is critical to design crystallization process based on the ternary phase diagram and avoid stable LL regions. Also, during an industrial crystallization process, LLPS is likely to occur when an anti-solvent is added to generate a supersaturated solution. LLPS preceding the addition of seeds can cause spontaneous nucleation of the API, which may not necessarily lead to the desired crystal form. Other issues that accompany LLPS include significant encrustation on reactor walls, poor impurity rejection, and loss of particle size control.

The most common way to mitigate LLPS is to switch to a different solvent system. However, these strategies are mostly based on trial-and-error. By leveraging an appropriate thermodynamic modelling tool, such as the SAFT-γ-Mie EoS, one can

simultaneously predict the crystalline solubility of the solute, and assess whether LLPS is predicted to occur. Even if an LLPS is predicted, then one can examine the phase diagram to determine whether the LLE binodal and SLE solubility curve are sufficiently separated so as to facilitate a crystallization process that avoids LLPS. In this way, the predictions serve as a screening tool to save time and resources.

If a solvent system has already been selected, and it is not desired to switch, one can also change the conditions applied in the crystallization process, such as temperature and solute concentration, to avoid the region(s) of the phase diagram where LLPS can occur. The latter approach requires measuring the LLPS phase boundary (or oiling-out limit) in the solvent system used for crystallization. Determining what regions of the diagram to explore can be guided by the aforementioned thermodynamic models. Effective ranges in temperature and solvent composition can then be outlined so that commercial operations can be carried out without crossing into the domain where LLPS occurs. In principle, one could also then use the experimental data to re-train the chosen model and thereby use model for quantitative process design.

Understanding stable and metastable LLPS is also important for the development of amorphous formulations. In such formulations, it is necessary to maintain the amorphous form of the drug to preserve its solubility and dissolution advantages. However, preventing crystallization can be challenging for some drugs.[38] Through proper formulation strategies, such as introducing a second drug as a fixed dose combination formulation or using an excipient that acts as an impurity or solvent to the API, the temperature where stable LLPS occurs may be lowered substantially, even down to room temperature. In this way, thermodynamically stable amorphous formulations can be prepared. The feasibility of this approach was demonstrated by the procaine–ethanol–heptane phase diagrams in this study, the previously reported spontaneous crystalline-to-amorphous transition of nifedipine,[36] and stable amorphous glassy solutions of several model drugs formulated with sucrose acetate isobutyrate that was recently reported.[39]

5. Conclusions

Both stable and metastable LLPS were observed for procaine in single and mixture solvents. In procaine–heptane binary systems, stable LLPS occurred at temperatures above the transition temperature T_{SLLE}, which was approximately 55 °C. Whereas in procaine–ethanol–heptane systems, stable LLPS occurred at temperatures well below the transition temperature identified for procaine–heptane alone. Five phase regions were identified below T_{SLLE}, including a homogeneous liquid phase, two stable solid–liquid regions, one stable solid–liquid–liquid region, and a stable liquid–liquid region. At 55 °C, only two phases remained, and all solid-containing phase regions disappeared, leaving only the homogenous liquid phase and a stable liquid–liquid equilibrium region. Prediction of the various phase equilibria was carried out using the state-of-the-art SAFT-γ-Mie EoS. This EoS was able to qualitatively reproduce highly complex phase behavior. While both the database model and the molecular model description of the solute (procaine) were explored, it was determined that regressing the crystalline solubility data (the molecular model) was necessary to obtain higher accuracy in the procaine–heptane system, but both approaches showed different strengths when predicting the procaine–ethanol–heptane phase behavior. The SAFT-γ-Mie EoS could be used as a screening tool to assess the propensity of solvent systems to oil-out, and also to predict phase diagrams for guiding experimentalist away from LLE regions in their crystallization process development. This study highlights the importance of quantitative understanding of the oiling-out behavior to successfully prevent oiling-out during crystallization and inhibit crystallization for amorphous formulations.

Abbreviations

API	Active pharmaceutical ingredient
GC/MS	Gas chromatography–mass spectrometry
HPLC	High-performance liquid chromatography
L	Liquid
LL	Liquid–liquid
LLE	Liquid–liquid equilibrium
LLPS	liquid–liquid phase separation
OOL	Oiling-out limit
PLM	Polarized light microscopy
SL	Solid–liquid
SLE	Solid–liquid equilibrium
SLL	Solid–liquid–liquid

Conflicts of interest

There are no conflicts to declare.

Acknowledgements

This study was supported by Boehringer Ingelheim Pharmaceuticals. The authors gratefully thank Dr. Capri Price in IMS for her assistance with GC/MS use. We also thank Pharm.D. student Shelly Evia for her assistance with some slurry experiments.

References

1 L. Myerson, *Handbook of Industrial Crystallization*, Butterworth-Heinemann 2nd edn, 2002.
2 N. G. Anderson, *Practical Process Research and Development*, Academic Press, 1st edn, 2000.
3 J. W. Mullin, *Crystallisation*, Butterworth Heinemann, 4th edn, 2002.
4 H.-H. Tung, E. L. Paul, M. Midler and J. A. McCauley, *Crystallization of organic compounds: an industrial perspective*, John Wiley & Sons, 2009.

5 L. Wang, Y. Bao, Z. Sun, V. J. Pinfield, Q. Yin and H. Yang, *Ind. Eng. Chem. Res.*, 2021, **60**, 4110–4119.
6 J. Lu, Y.-P. Li, J. Wang, Z. Li, S. Rohani and C.-B. Ching, *Org. Process Res. Dev.*, 2012, **16**, 442–446.
7 J. Lu, Y.-P. Li, J. Wang, G.-B. Ren, S. Rohani and C.-B. Ching, *Sep. Purif. Technol.*, 2012, **96**, 1–6.
8 G. S. Emilie Deneau, *Org. Process Res. Dev.*, 2005, **9**(6), 943–950.
9 D. B. Patience, P. C. Dell'Orco and J. B. Rawlings, *Org. Process Res. Dev.*, 2004, **8**, 609–615.
10 W. H. Lin, Z.-Q. Yu, P. S. Chow and R. B. H. Tan, *Crystals*, 2021, **11**, 1326.
11 L. Wang, H. Yang, Z. Sun, Y. Bao and Q. Yin, *Ind. Eng. Chem. Res.*, 2021, **60**, 18452–18463.
12 S. Kim, C. Wei and S. Kiang, *Org. Process Res. Dev.*, 2003, **7**, 997–1001.
13 K. Kiesow, F. Tumakaka and G. Sadowski, *J. Cryst. Grow.*, 2008, **310**, 4163–4168.
14 K. Li, S. Wu, S. Xu, S. Du, K. Zhao, L. Lin, P. Yang, B. Yu, B. Hou and J. Gong, *Ind. Eng. Chem. Res.*, 2016, **55**, 11631–11637.
15 L. Derdour, *Chem. Eng. Res. Des.*, 2010, **88**, 1174–1181.
16 P. E. Bonnett, K. J. Carpenter, S. Dawson and R. J. Davey, *Chem. Commun.*, 2003, 698–699, DOI: **10.1039/B212062C**.
17 S. Veesler, L. Lafferrère, E. Garcia and C. Hoff, *Org. Process Res. Dev.*, 2003, **7**, 983–989.
18 W. Beckmann, *Org. Process Res. Dev.*, 2000, **4**, 372–383.
19 E. Deneau and G. Steele, *Org. Process Res. Dev.*, 2005, **9**, 943–950.
20 H. Zhao, C. Xie, Z. Xu, Y. Wang, L. Bian, Z. Chen and H. Hao, *Ind. Eng. Chem. Res.*, 2012, **51**, 14646–14652.
21 M. Svärd, S. Gracin and Å. C. Rasmuson, *J. Pharm. Sci.*, 2007, **96**, 2390–2398.
22 J. Wang and D. R. Flanagan, *J. Pharm. Sci.*, 2002, **91**, 534–542.
23 H. Yang and Å. C. Rasmuson, *Org. Process Res. Dev.*, 2012, **16**, 1212–1224.
24 K. Ueda, K. Higashi and K. Moribe, *Mol. Pharmaceutics*, 2023, **20**(4), 1861–1871.
25 A. Alzghoul, A. Alhalaweh, D. Mahlin and C. A. Bergstrom, *J. Chem. Inf. Model.*, 2014, **54**, 3396–3403.
26 J. A. Baird, B. Van Eerdenbrugh and L. S. Taylor, *J. Pharm. Sci.*, 2010, **99**, 3787–3806.
27 V. Papaioannou, T. Lafitte, C. Avendano, C. S. Adjiman, G. Jackson, E. A. Muller and A. Galindo, *J. Chem. Phys.*, 2014, **140**, 054107.
28 S. Kashino, M. Ikeda and M. Haisa, *Acta Crystallogr., Sect. B: Struct. Crystallogr. Cryst. Chem.*, 1982, **38**, 1868–1870.
29 W. G. Chapman, K. E. Gubbins, G. Jackson and M. Radosz, *Fluid Phase Equilib.*, 1989, **52**, 31–38.
30 W. G. Chapman, K. E. Gubbins, G. Jackson and M. Radosz, *Ind. Eng. Chem. Res.*, 1990, **29**, 1709–1721.
31 V. Bhamidi and B. P. Abolins, *Processes*, 2019, **7**, 577.
32 S. Dufal, V. Papaioannou, M. Sadeqzadeh, T. Pogiatzis, A. Chremos, C. S. Adjiman, G. Jackson and A. Galindo, *J. Chem. Eng. Data*, 2014, **59**, 3272–3288.
33 L. S. Taylor and G. G. Z. Zhang, *Adv. Drug Delivery Rev.*, 2016, **101**, 122–142.
34 G. A. Ilevbare and L. S. Taylor, *Cryst. Growth Des.*, 2013, **13**, 1497–1509.
35 L. A. Sousa, S. M. Reutzel-Edens, G. A. Stephenson and L. S. Taylor, *Mol. Pharm.*, 2014, **12**, 484–495.
36 A. S. Indulkar, K. J. Box, R. Taylor, R. Ruiz and L. S. Taylor, *Mol. Pharmaceutics*, 2015, **12**, 2365–2377.
37 M. A. Lovette, J. Albrecht, R. S. Ananthula, F. Ricci, R. Sangodkar, M. S. Shah and S. Tomasi, *Cryst. Growth Des.*, 2022, **22**, 5239–5263.
38 J. Zha, *US Pat.*, 20140221424A1, 2014.
39 S. Dharani, K. Sediri, P. Cook, R. Arunagiri, M. A. Khan and Z. Rahman, *AAPS PharmSciTech*, 2021, **23**, 35.